Local measurements of screening currents driven by applied RMPs on TEXTOR

2014 Nucl. Fusion 54 064003

(http://iopscience.iop.org/0029-5515/54/6/064003)

IOP Publishing | International Atomic Energy Agency Nuclear Fusion
Nucl. Fusion **54** (2014) 064003 (9pp) doi:10.1088/0029-5515/54/6/064003

Local measurements of screening currents driven by applied RMPs on TEXTOR

P. Denner[1], Y. Liang[1], Y. Yang[2], M. Rack[1], L. Zeng[1,2], J. Pearson[1], Y. Xu[3] and the TEXTOR Team

[1] Forschungszentrum Jülich GmbH, Institute of Energy and Climate Research—Plasma Physics, EURATOM Association 52425 Jülich, Germany
[2] Institute of Plasma Physics, Chinese Academy of Sciences, 230031 Hefei, People's Republic of China
[3] Laboratoire de Physique des Plasmas—Laboratorium voor Plasmafysica, Association 'Euratom–Belgian state', École Royale Militaire—Koninklijke Militaire School, Trilateral Euregio Cluster, B-1000 Brussels, Belgium

E-mail: P.Denner@fz-juelich.de

Received 7 July 2013, revised 14 December 2013
Accepted for publication 23 January 2014
Published 23 May 2014

Abstract

In order to understand the mechanism by which resonant magnetic perturbations (RMPs) mitigate or suppress edge-localized modes, it is necessary to understand the plasma response to the application of RMPs. TEXTOR's fast movable Mirnov probe can provide direct measurements of the plasma response to RMPs applied using the dynamic ergodic divertor. The effect of toroidal plasma rotation is investigated, and a change in the phase of the plasma response at certain values of rotation is found. Jumps in the phase of the magnetic field are found to occur on resonant surfaces, indicating the formation of screening currents on these surfaces. The first observations of screening currents on multiple surfaces are presented, and the transition from screening to field penetration with increasing strength of the applied RMP field is observed.

Keywords: tokamaks, resonant magnetic perturbations, magnetic measurements

(Some figures may appear in colour only in the online journal)

1. Introduction

In order to avoid damage to plasma-facing components on ITER, type-I edge-localized modes (ELMs) must be either mitigated or suppressed [1]. The application of resonant magnetic perturbations (RMPs) to the plasma provides a promising method of ELM mitigation or suppression that has been successfully implemented to achieve complete suppression of type-I ELMs on DIII-D [2, 3] and mitigation of type-I ELMs on JET [4, 5], ASDEX Upgrade [6] and MAST [7, 8].

In the vacuum approximation, these RMPs cause the formation of magnetic islands and stochastic regions in the plasma edge. This introduces a radial component to parallel transport and therefore enhances radial transport, which leads to a reduction in the pedestal pressure gradient below the threshold value required to trigger ELMs. However, this description is incomplete since it does not include the effect of the plasma response to applied RMPs. For example, current sheets can form on rational surfaces and produce a magnetic field that locally cancels out the external perturbation, thus screening the RMPs. In addition, this vacuum description cannot explain ELM mitigation, whereby ELMs are destabilized and therefore occur more frequently (but are correspondingly smaller). Therefore, in order to understand the mechanism by which RMPs mitigate or suppress ELMs, it is necessary to understand the plasma response to the application of RMPs.

RMPs can be applied to TEXTOR plasmas using the dynamic ergodic divertor (DED) [9]. TEXTOR is also equipped with a fast movable Mirnov probe (FMMP) capable of measuring the magnetic field structure in the edge of TEXTOR plasmas with applied RMPs. By subtracting the vacuum magnetic field, direct measurements of the plasma response to RMPs can be obtained. The dependence of the plasma response on various parameters such as edge safety factor q_a, DED frequency f_{DED} and coil current I_{DED} has previously been reported in [10].

This paper presents an analysis of the direct measurements of the plasma response to applied RMPs on TEXTOR. An overview of the DED and FMMP systems used for the experiments is presented in section 2. This is followed by a presentation of the experimental results, which can be separated into two thrusts: the effect of toroidal plasma rotation

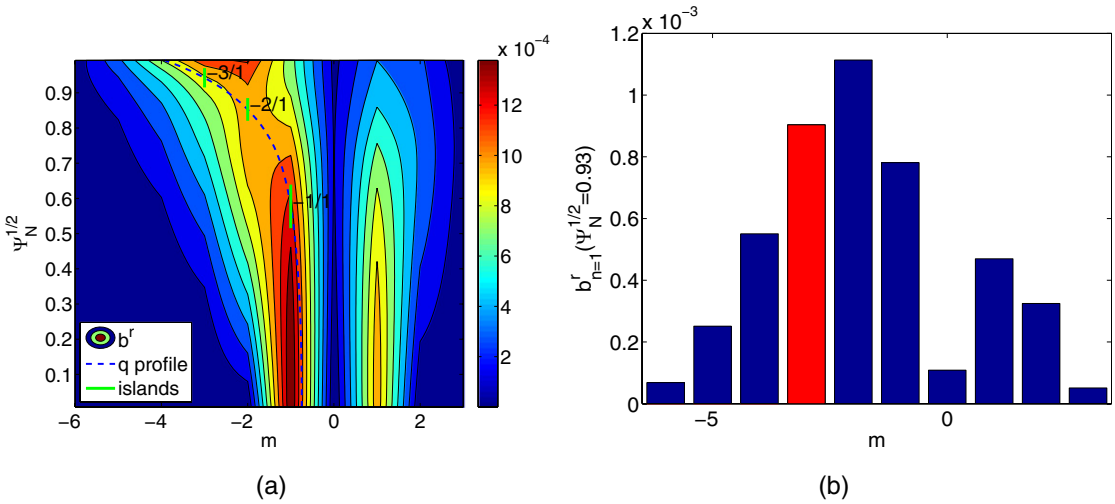

Figure 1. Perturbation spectrum for the $n = 1$ DED configuration (a) as a function of radius and (b) at a radius of $\Psi_N^{1/2} = 0.93$ in the plasma edge. The red bar indicates the resonant Fourier harmonic at this radius.

on the plasma response in section 3, and measurements of the magnetic field structure in the plasma edge in section 4. Section 5 provides a comparison of these results with previous work. Finally, a summary is given in section 6.

2. Experimental setup

TEXTOR is a medium-sized limiter tokamak with a circular cross-section. It has major radius $R_0 = 1.75$ m and minor radius $a = 47$ cm [11]. TEXTOR's DED consists of 16 helical coils on the high-field side (HFS) of TEXTOR capable of producing both ac and dc fields. Ac fields have the advantage that the induced plasma response has a known frequency—that of the DED field—and can therefore be distinguished from other modes in the plasma by means of a Fourier transform.

A unique feature of the TEXTOR DED is the ability to rotate the RMP field at frequencies comparable to that of the plasma rotation or MHD modes. The screening of RMPs as a result of plasma rotation is of particular interest. This rotational screening can arise from the motion of the electron fluid perpendicular to the field lines on a resonant surface. If the RMP field is rotating together with the electrons, then the RMP field is static in the reference frame of the electron fluid and screening is therefore not expected to occur [12]. The perpendicular electron velocity is the vector sum of the electron diamagnetic and $\boldsymbol{E} \times \boldsymbol{B}$ drift velocities. TEXTOR's rotating DED field makes it possible to investigate how effects of the applied RMPs vary with the difference between the rotation of the DED field and the rotation of the electron fluid.

The DED can be configured to produce fields with toroidal mode number $n = 1$ or $n = 2$. These configurations are conventionally referred to as $m/n = 3/1$ and $6/2$ respectively, although the DED coils do not produce fields with only one poloidal harmonic m. The perturbation spectrum for the $n = 1$ configuration is shown in figure 1. It can be seen that the dominant poloidal mode numbers are $m = 1$, $m = 2$ and $m = 3$. The results presented here were obtained with the DED in $3/1$ configuration. The DED frequencies that are available in this configuration are ± 1 and ± 5 kHz, where positive frequencies represent a rotation of the field in the counter-current (electron diamagnetic drift) direction and negative frequencies correspond to the co-current direction. The results for the ± 1 kHz case were obtained with DED coil currents up to $I_{\mathrm{DED}} = 2.0$ kA, whereas the current is limited to $I_{\mathrm{DED}} = 0.8$ kA for the ± 5 kHz case.

The FMMP is located at the midplane on the low-field side (LFS) of TEXTOR and can be plunged into the plasma edge in order to obtain radial profiles of the magnetic field. In the results presented here, the probe was plunged up to a maximum depth of $r = 40$ cm, i.e. 7 cm inside the plasma boundary. The probe can also be held at $r = 53$ cm, i.e. 6 cm outside of the plasma boundary, for the duration of a TEXTOR discharge. For hotter plasmas with NBI heating, this greatly reduces the risk of damage to the probe. The probe contains three groups of three Mirnov coils. Within every group, one coil is oriented in each of the radial, toroidal and poloidal directions so that every component of the magnetic field can be measured at three locations simultaneously. The three groups of coils have a separation of 0.5 cm in the radial direction (figure 2). During a plunge, only data recorded while the probe is being inserted are used, not while the probe is being withdrawn. This is because by the time the probe is withdrawn, it may have significantly perturbed the plasma.

An example of the measurements taken by the FMMP in a TEXTOR discharge can be seen in figure 3. This example is for a beam-heated plasma with NBI power $P_{\mathrm{NBI}} = 1.2$ MW, DED current $I_{\mathrm{DED}} = 0.8$ kA at a frequency of $f_{\mathrm{DED}} = +5$ kHz, toroidal field $B_{\mathrm{T}} = 1.6$ T, plasma current $I_{\mathrm{P}} = 250$ kA and line-averaged electron density $n_{\mathrm{e}} = 10^{19}$ m^{-3}. The data in this example is taken from the coil in the group closest to the plasma that measures the poloidal component of the magnetic field, B_θ. The measured field is correlated with the DED signal, and the Fourier component corresponding to the DED frequency is selected in order to distinguish the effect of the DED field from the background equilibrium plasma. The same is done for the magnetic field measured in a vacuum shot. This vacuum field is then subtracted from the data, so the effects of both the equilibrium plasma and the vacuum perturbation are removed from the measurements, and the remaining field is considered to be generated by the plasma as a response to the applied

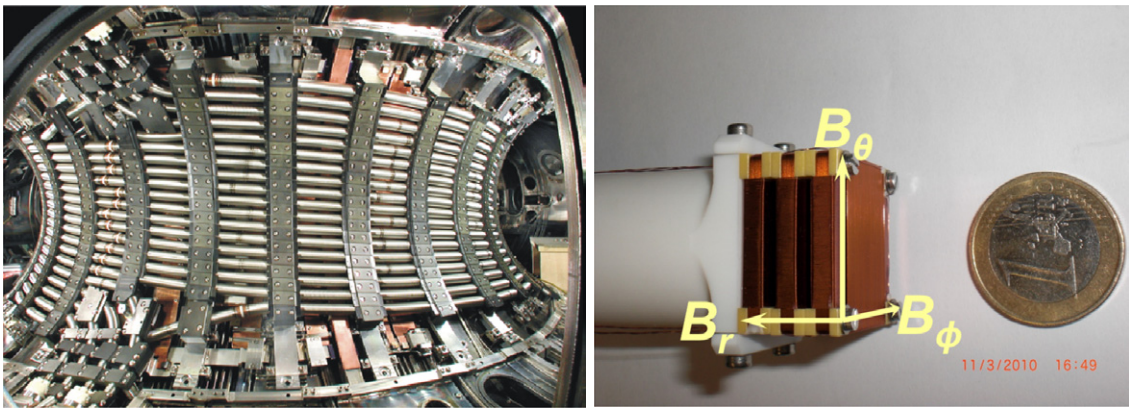

Figure 2. Photographs of (*a*) the DED coils and (*b*) the FMMP with its casing removed in order to show the three groups of coils inside. A € 1 coin is included for scale and the arrows show the directions in which each coil in a given group measures the local magnetic field.

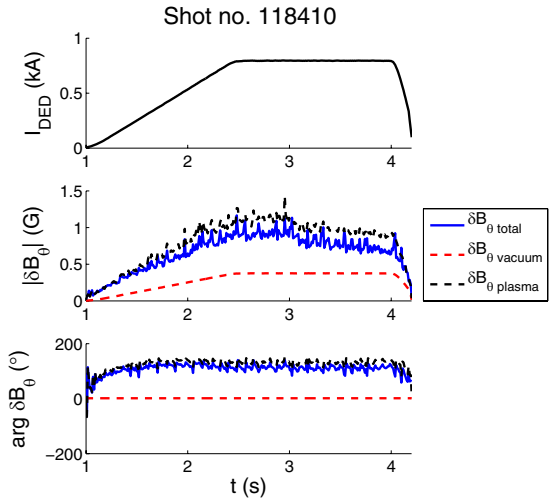

Figure 3. Measurements of the amplitude (middle) and phase (bottom) of $\delta B_{\theta\,\mathrm{plasma}}$, $\delta B_{\theta\,\mathrm{vacuum}}$ and $\delta B_{\theta\,\mathrm{total}}$ as the DED current (top) is ramped up, maintained at a constant value and then ramped down during a TEXTOR discharge. In this example, the position of the FMMP remains constant throughout the discharge at $r = 53$ cm.

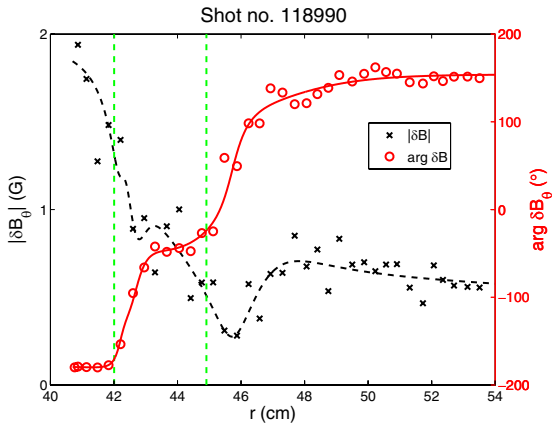

Figure 4. Radial profiles of the amplitude and phase of δB_θ recorded during a plunge of the FMMP. The vertical dashed lines show the location of the $q = 4$ and $q = 5$ surfaces from an equilibrium reconstruction calculated using the DIVA code.

RMPs. The middle and lower panels of the figure show the amplitude and phase of the fluctuating part of the poloidal field, $|\delta B_\theta|$ and $\arg \delta B_\theta$ respectively. The phase is defined relative to the DED field. In this example, the magnitude of $\delta B_{\theta\,\mathrm{total}}$, i.e. the sum of the vacuum field and the plasma response, is less than the magnitude of $\delta B_{\theta\,\mathrm{plasma}}$ on its own. This may seem counter-intuitive at first but can be understood by the fact that $\delta B_{\theta\,\mathrm{plasma}}$ has nearly the opposite phase to $\delta B_{\theta\,\mathrm{vacuum}}$. In this example, the probe remains outside of the plasma for the duration of the discharge.

When the probe is plunged into the plasma, radial profiles of the amplitude and phase of the plasma response such as those shown in figure 4 are obtained. The example shown is for an ohmic plasma with DED current $I_{\mathrm{DED}} = 1.3$ kA at a frequency of $f_{\mathrm{DED}} = -1$ kHz, toroidal field $B_{\mathrm{T}} = 1.6$ T, plasma current $I_{\mathrm{P}} = 180$ kA and line-averaged electron density $n_{\mathrm{e}} = 10^{19}\,\mathrm{m}^{-3}$. Two jumps are visible in the profile of the phase of δB_θ. The duration of the probe plunge is much longer than the DED time period, so many DED cycles occur during a single plunge. If probe measurements taken at different radial locations but at the same point in the DED cycle are compared, then any difference in the amplitude or phase of these measurements is most likely due to radial variation in δB. Therefore, if δB is plotted as a function of radius and time point in the DED cycle, radial variations in the amplitude or phase of δB should become apparent.

Figure 5 shows three examples of such plots. An example for a vacuum shot is shown in figure 5(*a*). In this case, there is no radial variation in the phase of the DED field, and since the FMMP on the LFS is located far from the DED coils on the HFS, the radial variation in the amplitude of the DED field is too small to be observed. Figures 5(*b*) and (*c*) show similar plots but with the addition of a TEXTOR plasma. In figure 5(*b*), there is a clear $\sim 180^\circ$ jump in the phase of δB_θ at $r \approx 45$ cm. This is interpreted as being caused by the presence of a screening current at this radial location, which should correspond to a resonant surface. Figure 5(*c*) shows no such phase jump, but a resonant surface is expected to exist within the range of r covered by the probe. This is interpreted as penetration of the RMP field and destruction of the screening current on this resonant surface.

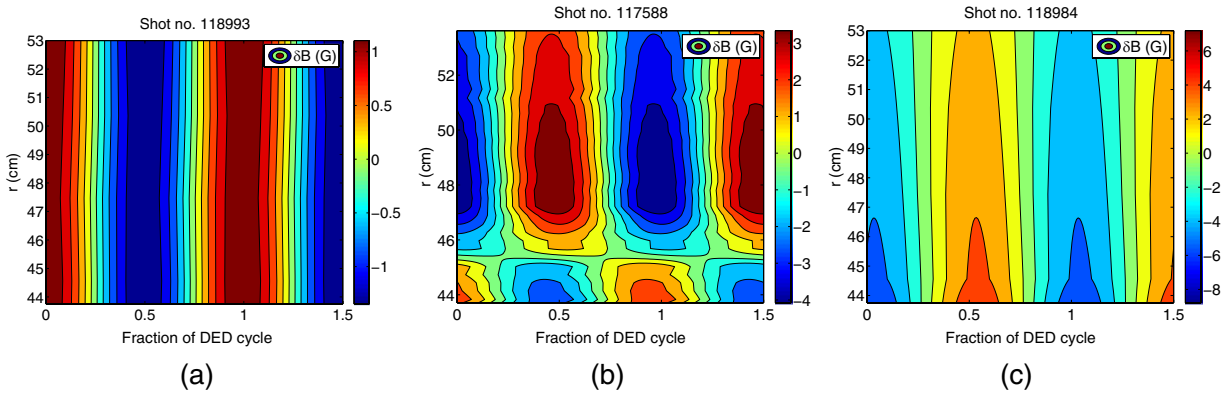

Figure 5. Example contour plots for (*a*) a vacuum shot, (*b*) screening and (*c*) penetration of the RMP field.

Given a radial profile of the amplitude and phase of δB_θ such as the one shown in figure 4, Ampère's law can be used to calculate the fluctuating part of the toroidal current density, δJ_ϕ, which in toroidal geometry is given by

$$\delta J_\phi = \frac{1}{\mu_0 r}\left(\frac{\partial}{\partial r}(r\delta B_\theta) - \frac{\partial}{\partial \theta}\delta B_r\right) \tag{1}$$

if the displacement current is neglected.

Although δB_r and δB_θ are similar in magnitude, it can be seen from figures 4 and 6(*a*) that radial changes in δB occur over distances of the order of a few centimetres. On the other hand, poloidal changes in δB should match the poloidal mode number m of the locally resonant harmonic of the perturbation field and therefore occur over distances of the order of $2\pi r/m$. For the $n = 1$ perturbations used in the work presented here, this corresponds to distances greater than 50 cm in the plasma edge, i.e. around an order of magnitude greater than the distances over which δB varies radially. Therefore, the poloidal derivative is neglected and (1) becomes

$$\delta J_\phi \approx \frac{1}{\mu_0 r}\frac{\partial}{\partial r}(r\delta B_\theta)\,. \tag{2}$$

In theory, δJ_θ could also be calculated from δB_ϕ using a similar equation. However, the magnitude of δB_ϕ is smaller than that of δB_θ, and the lower signal-to-noise ratio makes it difficult to fit a curve to the radial profile accurately enough to obtain meaningful values for δJ_θ. In any case, TEXTOR has a large aspect ratio $R_0/a \approx 3.7$, so δJ_θ is small in comparison to δJ_ϕ, assuming the screening current flows along magnetic field lines.

The amplitude and phase of δB_θ can equivalently be expressed as real and imaginary parts. Curves can be fitted to $\mathrm{Re}(\delta B_\theta)$ and $\mathrm{Im}(\delta B_\theta)$, from which radial profiles of $\mathrm{Re}(\delta J_\phi)$ and $\mathrm{Im}(\delta J_\phi)$ can be calculated using (1). In a similar way, the real and imaginary parts of δJ_ϕ can then be converted to amplitude and phase. This conversion adds no new information but helps with the intuitive understanding of the radial profile of δJ_ϕ. This whole process is outlined in figure 6. In figure 6(*c*), two clear peaks are visible in the radial profile of the amplitude of δJ_ϕ. This is evidence for the formation of current sheets on rational surfaces.

3. Effect of rotation on the plasma response

TEXTOR is equipped with one co-current and one counter-current neutral beam. By varying the relative power of the two beams while keeping the total NBI power constant, the toroidal plasma rotation can be varied with minimal changes to other plasma parameters, thus enabling the effect of the rotation on the plasma response to be investigated. No toroidal rotation measurements were available for the experiments presented here, but the NBI fraction f_{NBI}, which is a measure of the momentum input to the plasma, can be used as a proxy for toroidal rotation. The NBI fraction is defined in [13] as $f_{\mathrm{NBI}} = (P_{\mathrm{co}} - P_{\mathrm{counter}})/(P_{\mathrm{co}} + P_{\mathrm{counter}})$. Although no rotation measurements were available for these experiments, to give an idea of how values of the NBI fraction correspond to rotation values, in an earlier experiment for which rotation measurements were taken, albeit with different plasma parameters, as the NBI fraction was varied from $f_{\mathrm{NBI}} = -0.3$ to $f_{\mathrm{NBI}} = 1$, the plasma rotation varied approximately linearly from $\omega \approx -5\times10^4\,\mathrm{rad\,s^{-1}}$ to $\omega \approx 8\times10^4\,\mathrm{rad\,s^{-1}}$, with balanced beams producing a rotation of $\omega \approx -2\times10^4\,\mathrm{rad\,s^{-1}}$, where positive values of ω correspond to rotation in the co-current direction. The rotation could not be measured for $f_{\mathrm{NBI}} < -0.3$ since a minimum value of P_{co} was required for the rotation measurements.

Figure 7 shows the amplitude and phase of the radial and poloidal components of the plasma response to the RMP field as the NBI fraction is varied. This rotation scan was carried out with DED current $I_{\mathrm{DED}} = 0.8\,\mathrm{kA}$ at a frequency of $f_{\mathrm{DED}} = \pm5\,\mathrm{kHz}$, toroidal field $B_{\mathrm{T}} = 1.6\,\mathrm{T}$, plasma current $I_{\mathrm{P}} = 250\,\mathrm{kA}$ and line-averaged electron density $n_{\mathrm{e}} = 10^{19}\,\mathrm{m^{-3}}$. The FMMP was held at $r = 53\,\mathrm{cm}$. As mentioned in section 2, the electron diamagnetic drift occurs in the counter-current direction, which corresponds to the direction of rotation of the +5 kHz DED fields. For most of these plasmas, the phase of δB_θ is close to the phase of the vacuum field. However, when the +5 kHz DED field is applied to plasmas rotating in the co-current direction, there is a sharp change of phase, with the phase being nearly opposite for the $f_{\mathrm{NBI}} = 1$ case. As elaborated in section 4, this $\sim180^\circ$ change of phase suggests a transition between screening and field penetration. For $f_{\mathrm{NBI}} = 1$, a DED field rotating in the counter-current direction is applied to a plasma rotating in the co-current direction, and this large difference in rotation is likely to lead to strong

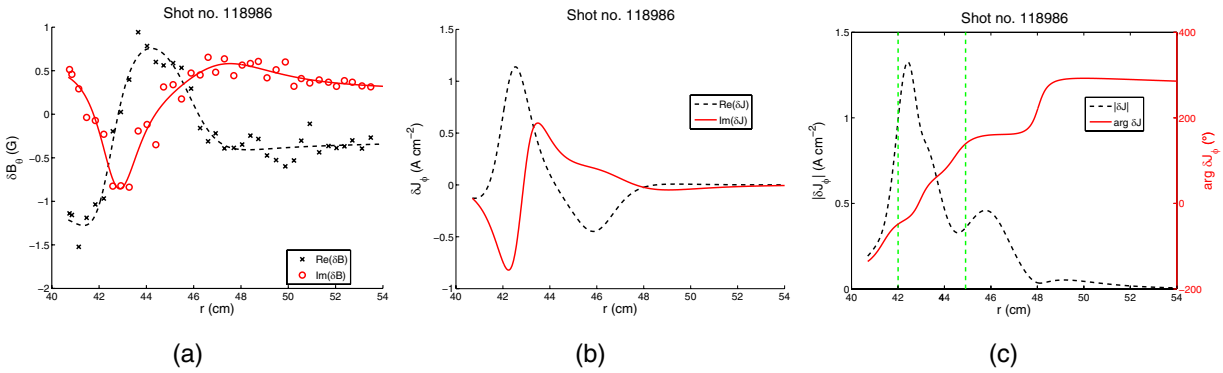

Figure 6. (*a*) Curves are fitted to radial profiles of δB_θ. These curves are then used to calculate δJ_ϕ in terms of (*b*) real and imaginary parts, and (*c*) amplitude and phase. In this example, two peaks in the amplitude of δJ_ϕ can be seen, corresponding to screening currents on two resonant surfaces. The location of the $q = 4$ and $q = 5$ surfaces from an equilibrium reconstruction calculated using the DIVA code are indicated by the vertical dashed lines.

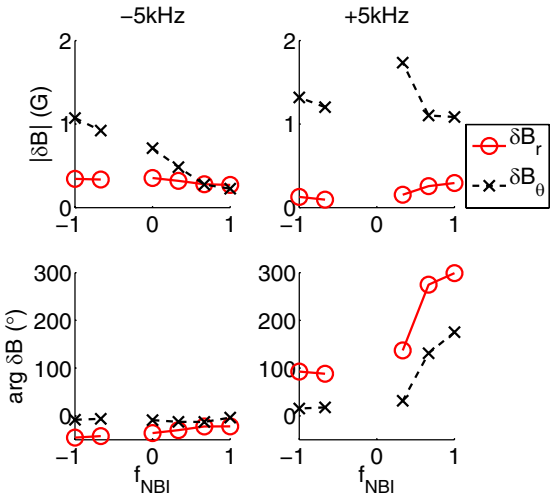

Figure 7. Amplitude (top) and phase (bottom) of the plasma response to applied RMPs as a function of NBI fraction for $f_{\mathrm{DED}} = -5$ kHz (left) and $f_{\mathrm{DED}} = +5$ kHz (right). The total NBI power was kept constant at 1.2 MW.

screening of the external field. However, no such phase change is observed when the −5 kHz DED field is applied to plasmas rotating in the counter-current direction.

The plots in figure 7 have a blank section, which corresponds to values of the NBI fraction for which the application of the DED leads to a disruption. An analysis of the data from an array of in-vessel Mirnov coils shows that for $f_{\mathrm{NBI}} = -\frac{1}{3}$, as soon as the DED current starts to ramp up, a 2/1 mode is triggered. This mode locks within ∼0.25 s for DED frequencies of both +5 and −5 kHz, and causes a disruption. For balanced beams, there is also a 2/1 mode. For $f_{\mathrm{DED}} = -5$ kHz, this mode does not lock, whereas for $f_{\mathrm{DED}} = +5$ kHz, it starts to lock ∼0.6 s after the DED current starts to ramp up. Once it starts to lock, the rotation braking is just as rapid as for $f_{\mathrm{NBI}} = -\frac{1}{3}$ and again causes a disruption.

4. Observation of screening currents

The first observations of multiple jumps in the phase of δB_θ in the same probe plunge are reported, which are interpreted as screening currents on multiple resonant surfaces. An example of this can be seen in figure 8(*a*), while figure 8(*b*) shows that these phase jumps are not observed in δB_r. This is consistent with the phase jumps being caused by screening currents flowing along field lines since phase jumps would only be expected in poloidal profiles of δB_r. Such poloidal profiles cannot be measured by the FMMP because it can only be plunged radially. The remainder of this article focuses on measurements of δB_θ.

Observations of screening currents on multiple resonant surfaces have been repeated for DED frequencies of ±1 and ±5 kHz. The observation of multiple resonant surfaces raises the possibility of observing overlapping surfaces or the formation of a stochastic region between surfaces. This would be more likely with the DED in 6/2 configuration since there would be more resonant surfaces and they would be closer together. Experiments in 6/2 configuration are included in future plans.

Figure 9 shows how the topology of the edge poloidal magnetic field changes as the DED current is increased with a frequency of $f_{\mathrm{DED}} = -1$ kHz. This DED current scan was carried out in ohmic plasmas with toroidal field $B_{\mathrm{T}} = 1.6$ T, plasma current $I_{\mathrm{P}} = 180$ kA and line-averaged electron density $n_{\mathrm{e}} = 10^{19}$ m^{-3}. At $I_{\mathrm{DED}} = 1.3$ kA, two ∼180° phase jumps are clearly visible, indicating the presence of screening currents.

An equilibrium reconstruction was carried out using the DIVA code in order to compare the radial location of these screening currents with the location of resonant surfaces in the equilibrium reconstruction. This equilibrium was found by solving the Grad–Shafranov equation using the core and edge plasma pressure, the toroidal field, the plasma current and the plasma geometry as input. Internal magnetic field measurements were not used for the equilibrium reconstruction, and there is some uncertainty in the location of the rational surfaces. However, TEXTOR equilibria produced using this method have previously been used in calculations of footprint patterns, which are highly sensitive to the location of rational surfaces in the plasma edge, and good agreement between modelling and experiment has been found [14, 15], suggesting that the error in the location of rational surfaces is less than 2–3 cm. Based on this equilibrium reconstruction, the two outermost surfaces are identified as the $q = 4$ and $q = 5$ surfaces (figure 10). In figures 4 and 6(*c*), it can be seen that the

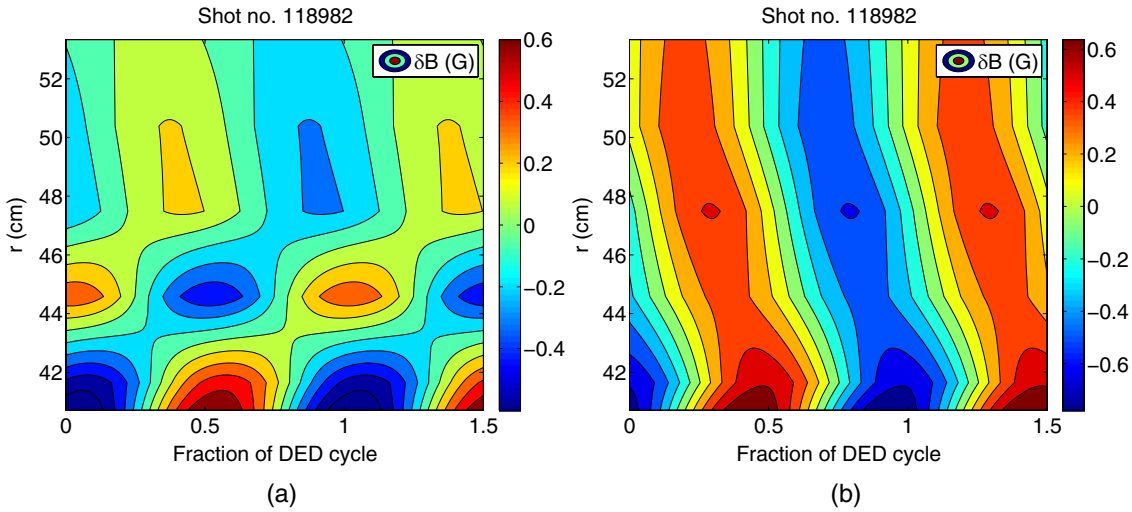

Figure 8. Contour plot of (*a*) δB_θ, showing an example of phase jumps across multiple resonant surfaces, and (*b*) δB_r for the same plasma, showing only a small, gradual phase change.

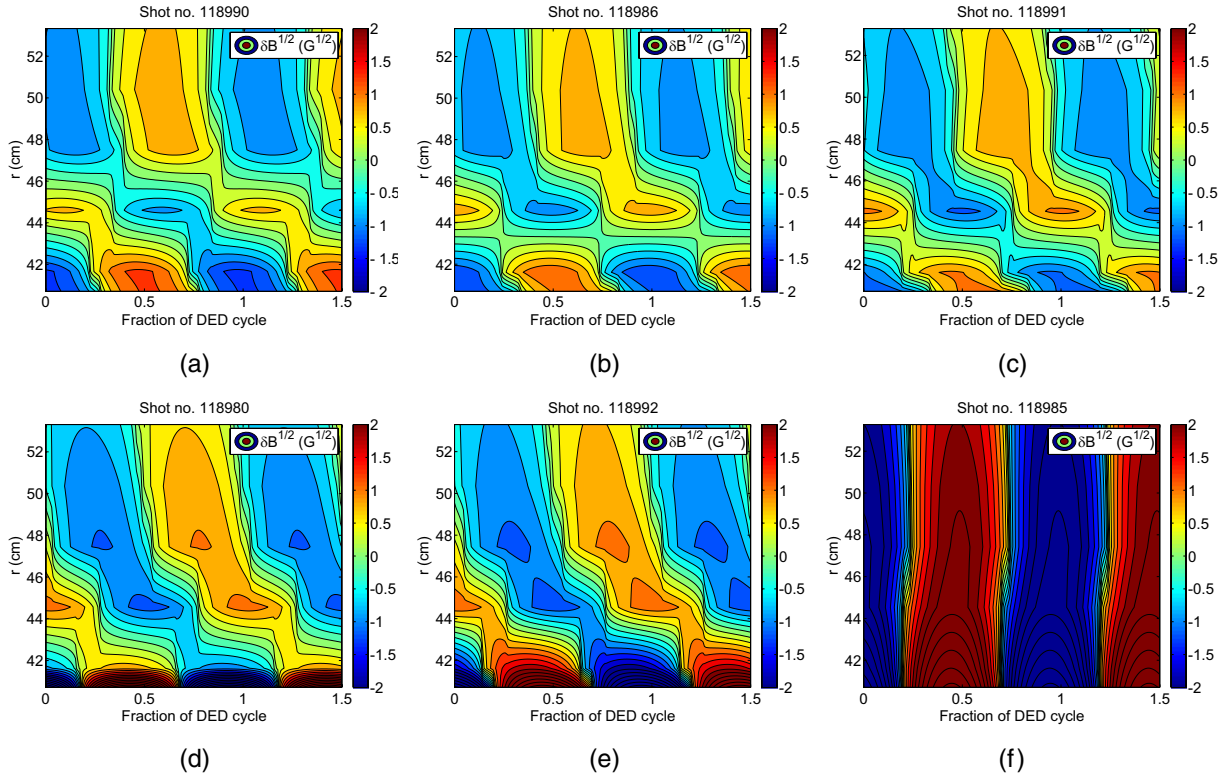

Figure 9. Topology of the edge poloidal magnetic field with a DED frequency of −1 kHz and current of (*a*) 1.3 kA, (*b*) 1.4 kA, (*c*) 1.5 kA, (*d*) 1.6 kA, (*e*) 1.7 kA and (*f*) 1.8 kA. $\delta B_\theta^{1/2}$ is plotted instead of δB_θ so that the same colour scale can be used for all of the plots without losing all of the detail for the plots with lower DED current and therefore lower values of δB_θ.

location of these surfaces does not exactly match the location of the maximum current density or the maximum gradient of the phase of δB_θ. However, the difference is not more than a centimetre, which is within the expected uncertainty.

As the DED current is increased, there is a gradual shift in the phase of δB_θ outside of the $q = 5$ surface such that the phase jump across the surface is reduced to $\sim 90^\circ$ at $I_{\mathrm{DED}} = 1.6$ kA. At this value of DED current, the amplitude of δB_θ begins to increase sharply inside the $q = 4$ surface. At $I_{\mathrm{DED}} = 1.8$ kA, the screening currents suddenly disappear and the amplitude of δB_θ suddenly increases throughout the plasma edge. An analysis of the data from an array of in-vessel Mirnov coils reveals that an $m/n = 2/1$ mode appears shortly after the DED current reaches its flat-top value of $I_{\mathrm{DED}} = 1.8$ kA. This 2/1 mode becomes locked to the DED frequency. It is possible that the DED current threshold for the penetration of the 2/1 mode is around 1.8 kA for $f_{\mathrm{DED}} = -1$ kHz. Another possibility is that penetration of the RMP field on the $q = 5$

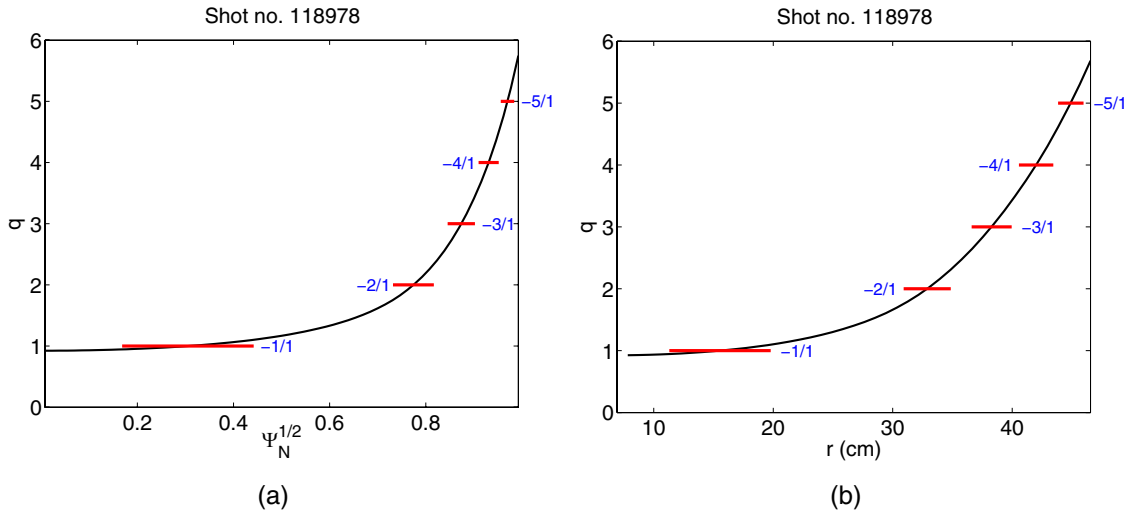

Figure 10. The q-profile for the plasma used in the DED current scan based on an equilibrium reconstruction using the DIVA code, plotted against (*a*) $\Psi_N^{1/2}$ and (*b*) minor radius r along the LFS midplane. The magnetic island widths as calculated using vacuum modelling are shown for the $I_{DED} = 1.3$ kA case. They clearly show the location of the resonant surfaces according to the equilibrium reconstruction.

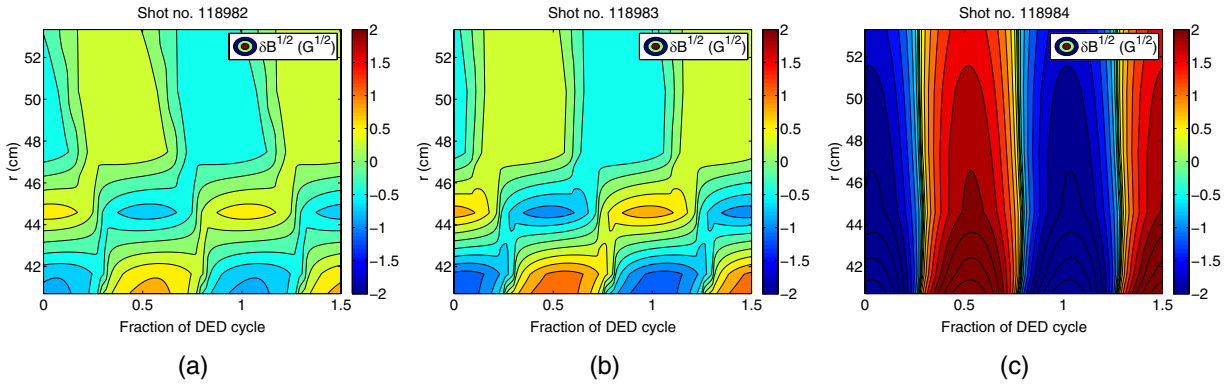

Figure 11. Topology of the edge poloidal magnetic field with a DED frequency of +1 kHz and current of (*a*) 0.4 kA, (*b*) 0.8 kA and (*c*) 1.2 kA.

surface, and perhaps also on the $q = 4$ surface, occurs first and leads to rotation braking, which then lowers the penetration threshold for the 2/1 mode. It could be the 2/1 mode that is responsible for the sudden increase in the amplitude of δB_θ at $I_{DED} = 1.8$ kA.

In a previous study, the reduced MHD code 4FC was used to model the plasma response to RMPs. A qualitative agreement with experimental measurements of the radial electric field on TEXTOR was found, but only when both the $m/n = 2/1$ and 3/1 harmonics of the perturbation field were included—when only the 2/1 harmonic was included, the results were qualitatively different from those obtained in the experiments. The 3/1 mode was found to be excited for any finite strength of the perturbation field, and the width of the 3/1 island was found to increase gradually with increasing perturbation amplitude. On the other hand, there was a threshold for the penetration of the 2/1 mode, but once this threshold was exceeded, the 2/1 island was found to grow very rapidly with increasing perturbation amplitude. At the same time, the MHD frequency for the 2/1 mode rapidly approached that of the DED frequency [16]. This is consistent with the gradual penetration of higher harmonics followed by the sudden penetration, growth and locking of a 2/1 mode.

Figure 11 shows a DED current scan carried out in ohmic plasmas with the same plasma parameters as above but with DED frequency $f_{DED} = +1$ kHz. The +1 kHz DED current scan was restricted to just three discharges because of the limited availability of experimental time. At $I_{DED} = 0.4$ and 0.8 kA, two resonant surfaces are observed. The contour plot for $I_{DED} = 1.2$ kA looks very similar to the 1.8 kA case for −1 kHz, i.e. the screening currents have disappeared and the amplitude of δB_θ is significantly increased. The data from the array of in-vessel Mirnov coils also reveal a similar 2/1 mode to that in the −1 kHz DED current scan. Therefore, it appears that the effect is similar but is obtained at lower values of DED current. This is expected since there is less difference between the rotation of the DED field and the rotation of the electron fluid. As in section 3, no rotation measurements were available for these plasmas. However, based on the earlier experiments with rotation measurements mentioned in section 3, it can be assumed that the intrinsic rotation in these ohmic plasmas is roughly similar to value of $\omega \approx 2 \times 10^4$ rad s^{-1} in the counter-current direction that was observed for balanced beams. The gradual shift in the phase of δB_θ outside the $q = 5$ surface has not been observed for $f_{DED} = +1$ kHz. However, this shift may occur at $0.8\,\text{kA} < I_{DED} < 1.2\,\text{kA}$.

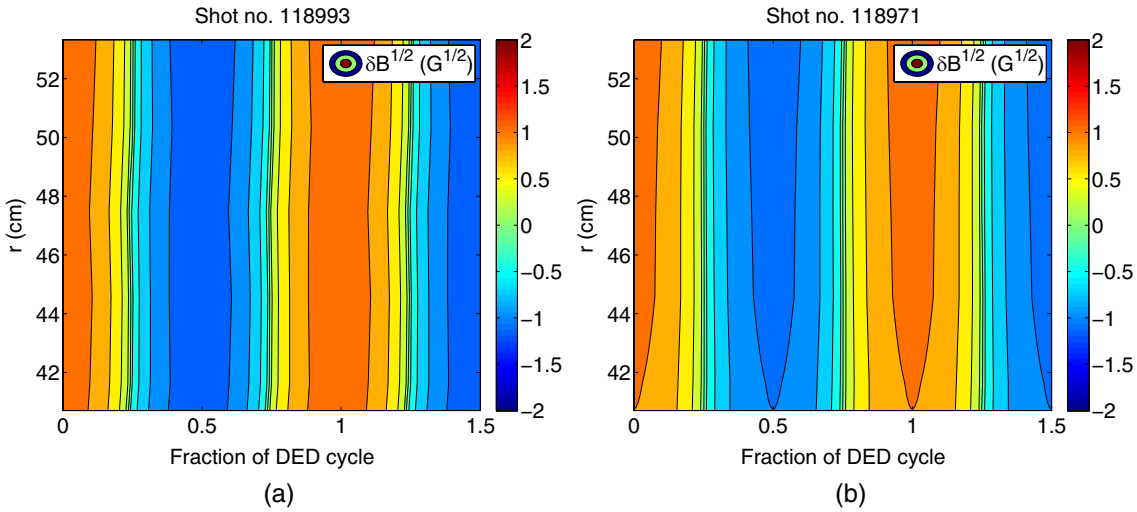

Figure 12. Vacuum reference shots for (a) −1 kHz and (b) +1 kHz DED current scans.

Since the perturbation field produced by the DED is applied on the HFS while the measurements are taken on the LFS, the phase of the measured δB_θ at a given location in the plasma may be expected either to match that of the DED field or to be inverted, depending on whether the poloidal mode number at this location is even or odd. In a previous study, this was indeed found to be the case when screening effects were dominant [10]. Figure 12 shows the vacuum reference shots for the DED current scans. By comparison with figures 9(a) and 11(a), where screening of the perturbation field is strongest, it can be seen that the phase of δB_θ outside of the surface with an even poloidal mode number, i.e. the $m/n = 4/1$ surface, is close to the phase of the vacuum field, whereas the phase outside of the surfaces with odd poloidal mode numbers, i.e. the $m/n = 3/1$ and $5/1$ surfaces, is nearly opposite to that of the vacuum field. It can also be seen that not only is the amplitude of the penetrated RMP field in figures 9(f) and 11 (c) significantly greater than the amplitude of the vacuum field but also that the phase differs by ∼180°. The presence of the 2/1 mode in these field penetration cases suggests that the perturbation field has penetrated at least up to the $q = 2$ surface. It is possible that the ∼180° phase shift relative to the vacuum field is a result of the outermost surface on which there is screening being the $m/n = 1/1$ surface, which has an odd poloidal mode number. However, since the FMMP cannot even come close to the $q = 1$ surface, the presence or absence of screening on this surface cannot be established with any certainty.

5. Comparison with previous work

In [17], fluctuations in the electron density n_e and temperature T_e were measured in the edge of TEXTOR plasmas with applied RMPs from the DED. A modulation of both n_e and T_e coherent to the DED frequency was observed but with a phase delay between n_e and T_e. This phase delay was interpreted as evidence of screening of the RMP field and was found to increase with increasing difference between the plasma rotation and the rotation of the DED field. This is consistent with the result in section 3 that the phase of δB relative to the vacuum field, which is also interpreted as evidence of screening of the RMP field, is large when the plasma is rotating in the co-current direction and the DED field is rotating in the counter-current direction.

Modelling of RMP fields using a drift-fluid model was presented in [18]. It was found that plasma response currents could form on resonant surfaces and screen the RMP fields. Screening currents in phase with the resonant component of the perturbation field on a rational surface were shown to be accompanied by currents that were 90° out of phase. These out-of-phase currents were found to be capable of having a strong impact on the magnetic field structure such that the phase of the resulting magnetic field could differ from that of the vacuum field. This is consistent with the results shown in section 4, where the magnetic field is also found to have a different phase from that of the vacuum field.

This modelling was extended in [19] using an analytical free energy minimization approach, and the effect of the strength of the RMP field on the screening was investigated. In section 4, at least for the −1 kHz case, the RMP field penetration is shown to occur very suddenly with a small increase in DED current. This very sudden field penetration may seem like a bifurcation. In fact, a bifurcation in RMP screening is predicted in [19] but only for low plasma resistivity, whereas the edge of a TEXTOR plasma is highly resistive. However, the prediction for high plasma resistivity is for an initial gradual reduction in screening with increasing RMP strength followed by a sudden drop, which is also consistent with the results presented here.

6. Summary and conclusions

This paper aims to investigate the plasma response to RMPs by directly measuring changes in the edge magnetic field that occur when RMPs are applied. A better understanding of the plasma response to RMPs is necessary in order to understand the mechanism behind ELM mitigation or suppression.

The effect of toroidal plasma rotation on the plasma response to RMPs has been investigated by varying the relative power of co- and counter-current NBI. A sharp change in the

phase of the plasma response is observed when co-current NBI is dominant and the DED field is rotating in the counter-current direction, which corresponds to a large difference between the rotation of the DED field and the rotation of the electron fluid. This phase change may be an indication of a transition between screening and field penetration.

The first observations of screening currents on multiple resonant surfaces have been made, and the transition from screening to field penetration with increasing DED current has been measured. As the DED current is increased, a gradual reduction in the phase jump across the outermost resonant surface occurs. As I_{DED} is increased further, there is an increase in the amplitude of the plasma response deeper inside the plasma followed by complete penetration of the RMP field. This initially gradual change followed by a very sudden field penetration is consistent with predictions from modelling [19]. After RMP field penetration, the fluctuating part of the magnetic field has a significantly greater amplitude and a $\sim 180^{\circ}$ phase difference compared to the vacuum case. This is possibly a result of the penetration of a $2/1$ mode. The threshold for RMP field penetration is found to be higher when the DED field rotates in the co-current direction, since in the absence of NBI heating, the electron fluid rotates in the counter-current direction and the difference in rotation frequency is therefore greater.

RMP modelling in the vacuum approximation does not include plasma parameters such as rotation or plasma response effects such as the formation of screening currents. These results highlight the importance of including such plasma parameters and plasma response effects when calculating the effect of RMPs.

It is only possible to insert the FMMP into relatively low-temperature L-mode plasmas, whereas ELM mitigation or suppression can only occur in ELMy H-mode plasmas. However, measurements could still be taken outside of an H-mode plasma. Therefore, in order to extend the relevance of this work to ELMy H-mode plasmas, a comparison between internal and external L-mode measurements is planned, which may be able to provide predictions of the internal magnetic field based on external measurements.

Further plans include the numerical implementation of screening currents as surface current sheets on resonant surfaces with amplitude and phase determined from experimental measurements as in figure 6. These current sheets can then be treated in the same way as RMP coils: the magnetic perturbation field that they produce can be calculated and superposed on the equilibrium field, hence island widths can be calculated and Poincaré plots can be produced in order to visualize the magnetic topology. This can then be used as an indication of whether overlapping islands or stochastic regions are formed. Further experiments are planned to be carried out with the DED in $m/n = 6/2$ configuration. This should provide a greater chance of observing overlapping islands or the formation of a stochastic region since there will be double the number of resonant surfaces with half the separation compared to the $3/1$ configuration. In addition, the possibility of carrying out a quantitative comparison with numerical simulation using existing two-fluid MHD models is currently under consideration.

Acknowledgments

The authors would like to thank their colleagues in the technical group (H. Jaegers, G. Satheeswaran, J. Aßman, S. Kraus, J. Thomas and others) for their substantial technical support. Support from the Helmholtz Association in the frame of the Helmholtz-University Young Investigators Group VH-NG-410 is gratefully acknowledged.

References

[1] Loarte A. *et al* 2003 *Plasma Phys. Control. Fusion* **45** 1549
[2] Evans T.E. *et al* 2004 *Phys. Rev. Lett.* **92** 235003
[3] Evans T.E. *et al* 2008 *Nucl. Fusion* **48** 024002
[4] Liang Y. *et al* 2007 *Phys. Rev. Lett.* **98** 265004
[5] Liang Y. *et al* 2010 *Nucl. Fusion* **50** 025013
[6] Suttrop W. *et al* 2011 *Phys. Rev. Lett.* **106** 225004
[7] Kirk A. *et al* 2011 *Plasma Phys. Control. Fusion* **53** 065011
[8] Kirk A., Chapman I.T., Harrison J., Liu Y.Q., Nardon E., Saarelma S., Scannell R., Thornton A.J. and the MAST Team 2013 *Plasma Phys. Control. Fusion* **55** 015006
[9] Finken K.H. 1997 *Fusion Eng. Des.* **37** 445
[10] Yang Y., Liang Y., Sun Y., Zhang T., Pearson J., Xu Y. and the TEXTOR Team 2012 *Nucl. Fusion* **52** 074014
[11] Samm U. 2005 *Fusion Sci. Technol.* **47** 73
[12] Nardon E., Tamain P., Bécoulet M., Huysmans G. and Waelbroeck F.L. 2010 *Nucl. Fusion* **50** 034002
[13] Koslowski H.R., Liang Y., Krämer-Flecken A., Löwenbrück K., von Hellermann M., Westerhof E., Wolf R.C., Zimmermann O. and the TEXTOR Team 2006 *Nucl. Fusion* **46** L1
[14] Jakubowski M.W., Abdullaev S.S., Finken K.H. and the TEXTOR Team 2004 *Nucl. Fusion* **44** S1
[15] Schmitz O. *et al* 2008 *Nucl. Fusion* **48** 024009
[16] Zhang T. *et al* 2012 *Nucl. Fusion* **52** 074013
[17] Stoschus H. *et al* 2010 *Phys. Plasmas* **17** 060702
[18] Reiser D. and Chandra D. 2009 *Phys. Plasmas* **16** 042317
[19] Reiser D. and Tokar M.Z. 2009 *Phys. Plasmas* **16** 122303